Asociación Argentina
de Mecánica Computacional

Mecánica Computacional Vol XXIX, págs. 5887-5911 (artículo completo)
Eduardo Dvorkin, Marcela Goldschmit, Mario Storti (Eds.)
Buenos Aires, Argentina, 15-18 Noviembre 2010

A 3D-1D-0D COMPUTATIONAL MODEL FOR THE ENTIRE CARDIOVASCULAR SYSTEM

Pablo J. Blanco[a,b] **and Raúl A. Feijóo**[a,b]

[a]*Laboratório Nacional de Computação Científica LNCC/MCT, Av. Getúlio Vargas 333, 25651-075 Petrópolis, Brazil, {pjblanco,feij}@lncc.br, http://www.lncc.br*

[b]*Instituto Nacional de Ciência e Tecnologia em Medicina Assistida por Computação Científica, Petrópolis, Brazil, http://macc.lncc.br/*

Keywords: closed-loop system, heterogeneous models, systemic circulation, cardiac circulation, valve models

Abstract. In the present work a computational model of the entire closed cardiovascular system is established. This model stands for the integration of different levels of circulation. Indeed, the arterial tree is described by a one dimensional model in order to simulate the propagation phenomena that takes place at the larger arterial vessels. The inflow and outflow locations of this 1D model are coupled with proper lumped parameter descriptions (0D model) of the remainder part of the circulatory system. At each outflow point we incorporate the peripheral circulation in arterioles and capillaries by using a 0D three-component Windkessel models. In turn, the whole peripheral circulation converges to the venous system through the upper and lower parts of the body, for which we set two corresponding major venous circulation circuits (superior and inferior vena cava). Then, the right and left heart circulation, as well as the pulmonary circulation are accounted for also by means of 0D models. Particularly for the four cardiac valves we employ a valve model allowing for the regurgitation phenomenon during the valve closing. Finally, the 0D model of the left ventricle is coupled with the inflow boundary in the 1D model, closing the system. In addition, we consider the existence of 3D models accounting for the detailed aspects of blood flow in specific vessels of interest. The resulting integrated model (3D-1D-0D coupled model) forms a closed loop network capable of taking into account the interaction between the global circulation (1D-0D Models) and the local hemodynamics (3D models). Several situations of interest are presented showing the capabilities of the model.

1 INTRODUCTION

The structural and functional behavior of the cardiovascular system can be considered as the result of the interplay among different levels of integration. Although such integration can sometimes be neglected, in some scenarios it allows the system to establish the way in which local and global phenomena are inter-related.

In the context of the modeling of the cardiovascular system, particularly in the present work, we identify some levels of integration: (i) the overall systemic behavior, (ii) the hemodynamics of large arteries, (iii) the local circulation in specific districts, (iv) the venous circulation and (v) the cardiac/pulmonary circulation. Such levels of integration are sometimes related to a certain geometrical scale (blood flow in large arteries), and sometimes are related to a given vascular entity (the heart).

Several models have been proposed in the literature in order to consider the relevant phenomena taking place at each level of integration, leading to the use of heterogeneous mathematical representations so as to account for the coupling of these levels of integration. As in the present work, in some cases the model chosen for a given level of integration is dictated by the information available, and in other cases this choice is made based on a trade-off between complexity and predictive capabilities.

In the literature there has been several approaches to integrate different levels of circulation in the sense introduced in the previous paragraphs. Mostly, models based on lumped representations were employed to accomplish this task Spencer and Deninson (1959); Schaaf and Abbrecht (1972); Liang and Liu (2005); Korakianitis and Shi (2006); Lanzarone et al. (2007); Reichold et al. (2009), incorporating 0D models to simulate flow in the larger arteries, veins and cardiac circulation. As well, distributed models for simulating the blood flow in compliant vessels has been an exhaustive area of research through the last decades Avolio (1980); Stettler et al. (1981); Kufahl and Clark (1985); Stergiopulos et al. (1992); Olufsen et al. (2000); Wang and Parker (2004); Reymond et al. (2009). More recently, 1D models of the arterial circulation have been coupled to 0D models of the venous-cardiac-pulmonary circulation Liang and Takagi (2009) to study the influence of arterial stenoses on the wave propagation. Particularly, the 1D model employed in Liang and Takagi (2009) was taken from Stergiopulos et al. (1992) and is comprised of 55 arterial segments and a 0D lumped representation for the peripheral/venous/pulmonary and cardiac circulations. In turn, valves are modeled using an ideal model of a diode, not allowing for backflow to occur. This last point has been addressed in Korakianitis and Shi (2006), in which phenomenological models of the cardiac valves are proposed in order to model more accurately the openin and closing phased of the valves, being allowed to model certain pathological conditions like valve regurgitation and stenosis.

In the field of modeling blood flow in specific vessels, several works have dealt with the use of heterogeneous representations in order to couple local and global hemodynamics phenomena. This has been mostly carried out using 3D and 1D (or 0D) models to couple blood flow in complex arterial geometries with either full or partial models for the systemic dynamics Formaggia et al. (2001); Blanco et al. (2007); Vignon-Clementel et al. (2006); Urquiza et al. (2006); Grinberg et al. (2009); Migliavacca et al. (2006); Blanco et al. (2009); Kim et al. (2009); Blanco et al. (2010).

In the context introduced in the previous paragraphs, this work presents a computational model of the entire cardiovascular system borrowing the most important features of the different models available in the literature. Thus, the model introduced here for the cardiovascular system has more descriptive capabilities than the models currently available in the literature.

Indeed, it allows to accounts for specific vessels, systemic arteries, systemic veins, pulmonary and heart circulation and complex valve functioning. Rather than multiscale modeling of the cardiovascular system in this case we refer to *integrative modeling* of the cardiovascular system. In the present approach, the arterial tree is described by a one dimensional model with 128 arterial segments, following Avolio (1980), in order to simulate the propagation phenomena that takes place at the larger arterial vessels. The inflow and outflow locations of this 1D model are coupled with proper lumped parameter descriptions (0D model) of the remainder part of the circulatory system. At each outflow point we incorporate the peripheral circulation in arterioles and capillaries by using 0D three-component Windkessel models, following Stergiopulos et al. (1992). In turn, the whole peripheral circulation converges to the venous system through the upper and lower parts of the body (following Liang and Takagi (2009)). These two main compartments are represented using lumped models for the venules, veins and cavas (inferior and superior). The right and left heart circulation, as well as the pulmonary circulation are also modeled by means of 0D models. Particularly we point out the modeling of the four heart valves, which is carried out by using a non-linear model which allows for the regurgitation phase during the valve closing following Korakianitis and Shi (2006). Finall, the 0D model of the left ventricle is coupled with the inflow boundary in the 1D model, closing the cardiovascular loop. The entire 0D model which performs the coupling between the outflow and inflow points in the arterial tree consists of 14 compartments. Following Blanco et al. (2007, 2009, 2010), we can consider the existence of 3D models accounting for all the complexity of three-dimensional blood flow in specific vessels of interest. The resultant integrated model (0D-1D-3D coupled model) forms a closed loop network capable of taking into account the interaction between the global circulation (0D-1D models) and the local hemodynamics (3D models). In order to sum up, this is carried out by putting together the following mathematical representations

(a) 1D Models for the larger systemic arteries;

(b) 0D Models (R/C windkessel models) for the arterioles and capillaries;

(c) 0D Models ($R/L/C$ models) for venules and veins to model the upper and lower body parts;

(d) 0D Models ($R/L/C$ models) for inferior and superior vena cava, pulmonary veins and pulmonary arteries;

(e) 0D models (elastance models) for each of the four heart chambers;

(f) 0D Models (non-linear non-ideal diode models) to approximate the behavior of the tricuspid, pulmonary, mitral (bicuspid) and aortic valves;

(g) 3D Models for the specific vessels of interest.

With the model for the cardiovascular system presented here there is open field to incorporate homeostatic mechanisms so as to allow the system to perform self-regulation, with which its predictability is considerably augmented.

This work is organized as follows. Section 2 presents all the mathematical representations used in this work for the different levels of circulation. In Section 3 all the representations are written within the context of the integrative model of the cardiovascular system. Section 4 provides the data upon which our model is based. In Section 5 the model is employed to simulate different cardiovascular scenarios involving such heterogeneous models. The final remarks are given in Section 6.

2 MATHEMATICAL MODELS FOR THE VASCULAR ENTITIES

2.1 1D model for the systemic arteries

The arterial blood flow (item (a) in the list of Section 1) is modeled as the flow of a fluid in 1D compliant vessels to be able to capture the wave propagation phenomena and its non-linear features. Therefore, the governing equations for the 1D portion of the arterial system (all the arterial segments) are derived from the Navier-Stokes equations by introducing suitable assumptions. This procedure yields the following set of partial differential equations (see Hughes (1974) for its derivation)

$$\frac{\partial Q}{\partial t} + \frac{\partial}{\partial x}\left(\beta \frac{Q^2}{A}\right) = -\frac{A}{\rho}\frac{\partial P}{\partial x} - \frac{\pi D}{\rho}\tau_o, \tag{1}$$

$$\frac{\partial A}{\partial t} + \frac{\partial Q}{\partial x} = 0, \tag{2}$$

with

$$\tau_o = f_r \frac{\rho \tilde{u}|\tilde{u}|}{8} \qquad Q = \tilde{u}A, \tag{3}$$

where A is the cross sectional area of the artery (D its diameter), $\tilde{u}$ the mean value of the axial velocity, x the axial coordinate, P the mean pressure, ρ the blood density, τ_o the viscous shear stress acting on the arterial wall, f_r a Darcy friction factor (in this work a fully developed parabolic velocity profile is considered) and β is the momentum correction factor ($\beta = 1$ is considered here).

The system is closed by introducing a constitutive law which establishes a relation between the pressure and the cross sectional area. Here the following visco-elastic model Kivity and Collins (1974b,a) is used

$$P = P_{\mathrm{o}} + \frac{E h_{\mathrm{o}}}{R_{\mathrm{o}}}\left(\sqrt{\frac{A}{A_{\mathrm{o}}}} - 1\right) + \frac{K h_{\mathrm{o}}}{R_{\mathrm{o}}}\frac{1}{2\sqrt{A_{\mathrm{o}} A}}\frac{\partial A}{\partial t}, \tag{4}$$

being R the radius of the artery, E an effective Young modulus, K is the viscosity of the wall, h the thickness of the arterial wall and the subscript 'o' denotes quantities evaluated at the reference pressure P_{o}. More complex arterial wall models can to be considered, like models accounting for collagen fibers. This is not treated in the present work.

In this model we may identify two weak points which give us room for improvement:

- the friction term is derived from the assumption of a fully developed parabolic velocity profile;
- the momentum correction factor is derived from the assumption of a fully developed flat velocity profile.

Regarding these two points the interested reader is referred to Kufahl and Clark (1985); Reymond et al. (2009) for two different approaches to improve the capabilities of the model.

2.2 0D model for the arterioles and capillaries

The peripheral circulation (item (b) in the list of Section 1) is represented through Windkessel models Stergiopulos et al. (1992); Schaaf and Abbrecht (1972). The Windkessel behaviour is determined by a resistance R_c to represent the capillaries, in series with the parallel of a

resistance R_a and a capacitor C_a to model the arterioles, as can be seen in Figure 1, where P_i and P_o are the pressures at the input and output of the compartment, respectively, Q_i and Q_o are the blood inflow and outflow, respectively.

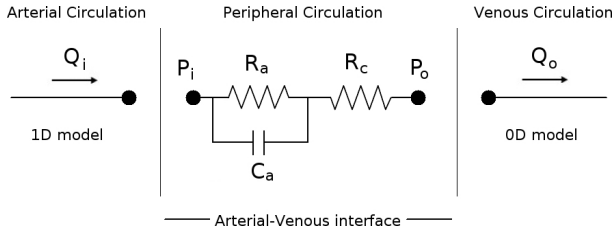

Figure 1: The 0D Windkessel model for the peripheral circulation.

The balance equations for this model are the following

$$\frac{dQ_i}{dt} = \frac{1}{R_c R_a C_a}\left[R_a C_a \frac{d}{dt}(P_i - P_o) + (P_i - P_o) - (R_c + R_a)Q_i\right], \tag{5}$$

$$Q_i = Q_o. \tag{6}$$

The Windkessel element is an interface arterial-venous model. Thus the P_i is the pressure from the arterial side (at the input of the compartment) while P_o is the pressure from the venous side (at the output of the compartment), more precisely at the venules.

2.3 0D model of the venous and pulmonary circulation

The models to simulate the blood flow through the venules, veins, superior and inferior vena cava and also the pulmonary arteries and pulmonary veins (items (c)-(d) in Section 1) are mathematically formulated in terms of an electric analog model in which inertial effects are considered. A single compartment is represented in Figure 2 in which R and L denote the resistance and inertance of the circuit, respectively; C the compliance of the compartment, P_i and P_o are the pressures at the input and output of the compartment, respectively, P_{ex} is the external pressure which also could be a function of time and, finally, Q_i and Q_o are the blood inflow and outflow, respectively, into the compartment.

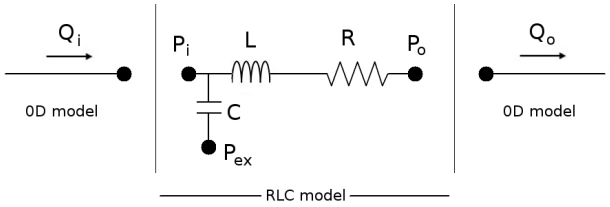

Figure 2: Single-compartment circuit representation.

The governing equations associated to this generic single compartment are given by

$$L\frac{dQ_o}{dt} + RQ_o = P_i - P_o, \tag{7}$$

$$C\frac{d}{dt}(P_i - P_{ex}) = Q_i - Q_o, \tag{8}$$

for the case when C is constant. We specified the external pressure P_{ex} as, for example, the intrathoracic pressure that during normal respiration varies between approximately -4 and

$-6mmHg$. A simple sinusoidal variation between these two values may be assumed at a respiratory frequency of 12 breaths/min.

2.4 0D model for the heart and valves

The whole cardiac circulation is divided into two halves. Each half consists of two chambers and two valves. We divide the presentation here in order to separate the balance equations at the cardiac chambers and at the heart valves. The part of the model presented here is also written using 0D lumped models (items (e)-(f) in Section 1). The electric analog model for the valves presented here corresponds to a non-ideal diode (see Figure 3).

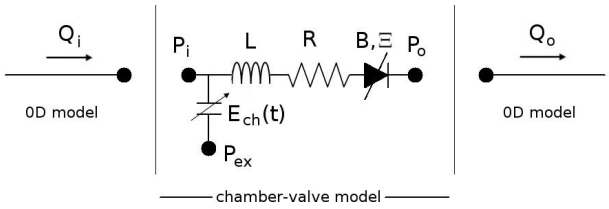

Figure 3: Generic chamber-valve element with a non-ideal diode.

The model shown in Figure 3 is composed by a inertance, resistance and flow separation terms, but the model also incorporates the partial states of the diode through another state variable called Ξ. This additional variable takes into account non-binary states of the valve.

2.4.1 Elastance model for the cardiac chambers

Elastance-based modeling of the heart has been adopted in this study to describe each of the four cardiac chambers. Based on the elastance model, blood pressure in each cardiac chamber, denoted by P_i, is given by

$$P_i - P_{ex} = E_{ch}(t)(V_{ch} - V_{0,ch}) + S_{ch}\frac{dV_{ch}}{dt}, \tag{9}$$

where V_{ch} is the cardiac volume of the chamber and $V_{0,ch}$ refers to the dead volume of such chamber, S_{ch} is the viscoelasticity coefficient for the cardiac wall chamber, which is related linearly to the cardiac pressure through the expression (see Liang and Takagi (2009))

$$S_{ch} = \alpha_{ch}|P_i|. \tag{10}$$

In turn, E_{ch} is given by

$$E_{ch}(t) = E_A e(t) + E_B, \tag{11}$$

where E_A is the amplitude of elastance, E_B is the baseline value of elastance, and $e(t)$ is a normalized time-varying function of the elastance, which for ventricles is

$$e_v(t) = \begin{cases} \frac{1}{2}\left[1 - \cos\left(\pi\frac{t}{T_{vc}}\right)\right] & 0 \le t \le T_{vc} \\ \frac{1}{2}\left[1 + \cos\left(\pi\frac{(t - T_{vc})}{T_{vr}}\right)\right] & T_{vc} < t \le T_{vc} + T_{vr} \\ 0 & T_{vc} + T_{vr} < t \le T \end{cases} \tag{12}$$

and for atria is

$$e_a(t) = \begin{cases} \frac{1}{2}\left[1+\cos\left(\pi\frac{(t+T-t_{ar})}{T_{ar}}\right)\right] & 0 \le t \le t_{ar}+T_{ar}-T \\ 0 & t_{ar}+T_{arp}-T < t \le t_{ac} \\ \frac{1}{2}\left[1-\cos\left(\pi\frac{(t-t_{ac})}{T_{ac}}\right)\right] & t_{ac} < t \le t_{ac}+T_{ac} \\ \frac{1}{2}\left[1+\cos\left(\pi\frac{(t-t_{ar})}{T_{ar}}\right)\right] & t_{ac}+T_{ac} < t \le T \end{cases} \tag{13}$$

Here, the subscript v denotes the ventricles, and a the atria, T is the duration of a cardiac cycle, T_{vc}, T_{ac}, T_{vr} and T_{ar} refer to the durations of ventricular/atrial contraction/relaxation, and t_{ac}, t_{ar} the times when the atria begin to contract and relax, respectively.

Finally, the volume is related to the inflow and outflow as usual

$$\frac{dV_{ch}}{dt} = Q_i - Q_o. \tag{14}$$

2.4.2 Non-ideal diode model for the heart valves

The momentum balance in each heart valve is such that we take into account the non-linear behavior by which the flow can be inverted when the valve closes. The model employed also accounts for intertial and resistive components and it has been inpired in the valve model presented in Korakianitis and Shi (2006). With such model it is possible to simulate different scenarios including normal and abnormal regurgitation, as well as valve stenosis. Hence, the governing equation is the following

$$L\frac{dQ_o}{dt} + RQ_o + B|Q_o|Q_o = \Xi(P_i - P_o), \tag{15}$$

where L is the inertance of the fluid, R is the viscous resistance, B accounts for the flow separation phenomenon and P_i and P_o are the input and output pressure values in the compartment. The non-binary state of the valve is considered through the coefficient Ξ. This coefficient simulates the behavior of the orifice of the valve, and is a function of the opening angle of the valve, denoted by θ, as follows

$$\Xi = \frac{(1-\cos\theta)^4}{(1-\cos\theta_{max})^4}. \tag{16}$$

where θ_{max} is the maximum angle the valve is able to open. Therefore, an equation for θ must be provided, and this is done by using an angular momentum balance for the valve. This equation balances the angular acceleration of the valve with several angular momenta, namely: due to the gradient pressure gradient M_P, due to friction M_F, due to blood velocity M_Q and due to downstream vortex formation M_V. Hence, such equation reads (see Korakianitis and Shi (2006) for more details) as follows

$$I\frac{d^2\theta}{dt^2} = M_P + M_F + M_Q + M_V, \tag{17}$$

where I is the momentum of inertia of the valve, and all the momenta are given as

$$M_P = k_P(P_i - P_o)\cos\theta, \tag{18}$$

$$M_F = -k_F\frac{d\theta}{dt}, \tag{19}$$

$$M_Q = k_Q Q_o \cos\theta, \tag{20}$$

$$M_V = \begin{cases} k_V Q_o \sin(2\theta) & \text{if } P_i \geq P_o, \\ 0 & \text{if } P_i < P_o. \end{cases} \tag{21}$$

The solution of this balance equation must consider the maximum and minimum angles the valve is able to reach. That is, equation (17) is complemented with the following restrictions

$$\theta = \begin{cases} \theta_{min} & \text{if } \theta < \theta_{min}, \\ \theta_{max} & \text{if } \theta > \theta_{max}. \end{cases} \tag{22}$$

In this way, a valve can undergo malfunctioning in either of two distinct ways (or combination of them). These are *stenosis* if the valve is narrowed, and *incompetence* or *insufficiency* when the valve is leaky and fails to prevent prominent backward flow. In particular, both situations are easily modeled using the previous equation. A stenosed valve is modeled restricting the maximum opening angle θ_{max}, whereas an incompetent valve is modeled by setting a larger value for θ_{min}.

2.5 3D model for specific vessels

The Navier-Stokes equations in moving domains (ALE formulation) are employed for describing the blood flow in specific arterial vessels (item (g) in Section 1). Then, the equations are

$$\rho\frac{\partial \mathbf{u}}{\partial t} + \rho\left(\mathbf{u} - \mathbf{v}\right)\nabla\mathbf{u} - \mu\triangle\mathbf{u} + \nabla P = \mathbf{f}, \tag{23}$$

$$\text{div } \mathbf{u} = 0, \tag{24}$$

$$+ \text{ proper coupling conditions (see Section 3) at } \Gamma_i \quad i = 1, \ldots, N_{cf}, \tag{25}$$

where $\mathbf{u}$ is the fluid viscosity, $\mathbf{v}$ is the velocity of the frame of reference consistent with the ALE formulation, P is the pressure field, $\mathbf{f}$ is the volume body force, ρ and μ are density and viscosity, respectively, and Γ_i, $i = 1, \ldots, N_{cf}$, are the interfaces in the 3D model which are to be coupled with the 1D model of the arterial tree. This set of equations must be provided with proper boundary conditions and a proper constitutive relation relating the displacement of the arterial wall with the pressure (structural model). As in our previous works, we choose an independent rings wall model consistent to that used for the 1D model. In this manner, the following equations are used for the surface points in $\partial\Omega_w$ -the surface representing the arterial wall-

$$P - P_{\text{o}} = \frac{Eh_{\text{o}}}{R_{\text{o}}^2}\delta + \frac{kh_{\text{o}}}{R_{\text{o}}^2}\frac{d\delta}{dt} \tag{26}$$

$$\mathbf{w} = \delta\,\mathbf{n} \tag{27}$$

$$\mathbf{v} = \frac{\partial \mathbf{w}}{\partial t} \tag{28}$$

where δ is the displacement of the nodes placed on the arterial wall normal to the surface ($\mathbf{n}$ is the normal vector to the surface), $\mathbf{w}$ is the displacements vector for the deformable domain with respect to its reference configuration, which is extended to the interior of the domain by solving the problem $\triangle \mathbf{w} = 0$. It is evident the analogy between the equation (26) to that given in (4) for the 1D model.

Other constitutive behaviors for the blood can be incorporated in the model, giving rise to an equation similar to (23) but now valid for non-Newtonian fluids, like the one obtained when the regularized Casson model is used.

3 ENTIRE COUPLED MODEL

The entire model can now be described step-by-step. It is schematically shown in Figure 4. The glossary of the terms used in Figure 4 is given in Table 1. In this table N_{sa} denotes the total number of systemic arteries employed and N_{wlb} and N_{wub} are the number of Windkessel models pertaining to the lower and upper parts of the body, respectively, with $N_w = N_{wlb} + N_{wub}$ the total number of Windkessel elements in the arterial side.

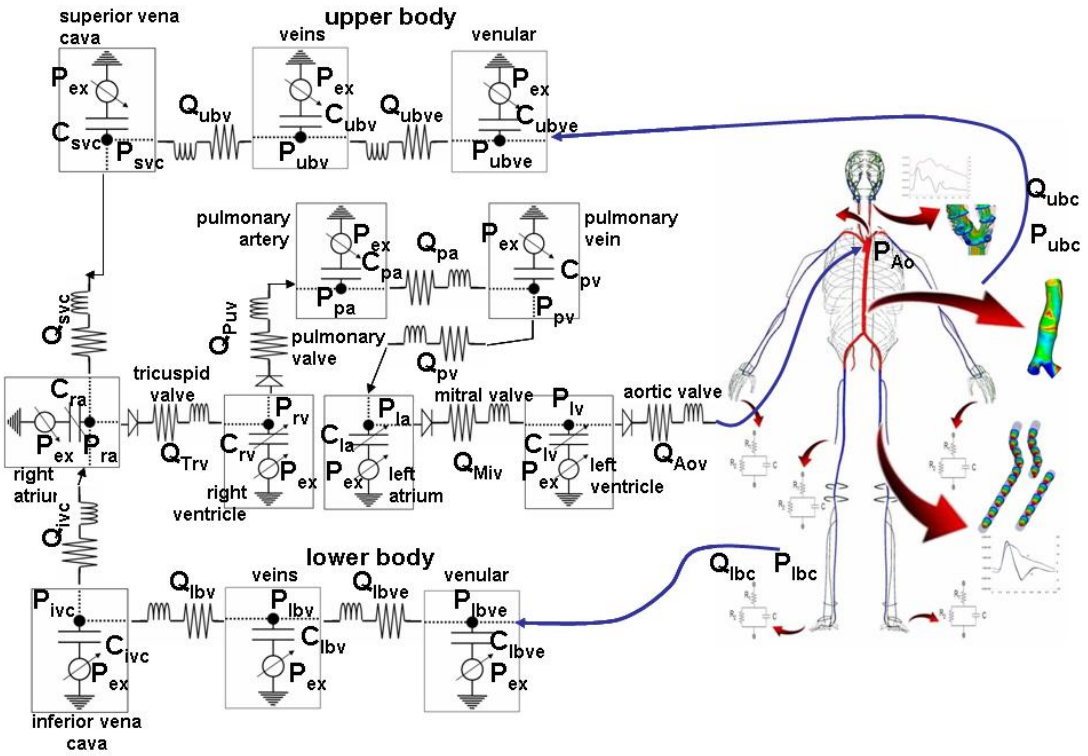

Figure 4: Entire closed loop model of the cardiovascular system.

We start at the aortic root until reaching it again closing the loop:

Larger Arteries. From the aortic root to the smaller arteries the 1D model described by equations (1), (2) and (4), that is, for each one of the N_{sa} arteries present in the model we

sa,m:	systemic arteries, $m = 1, \ldots, N_{sa}$
w,k:	Windkessel models, $m = 1, \ldots, N_w$
wlb,k:	lower body Windkessel models, $k = 1, \ldots, N_{wlb}$
wub,k:	upper body Windkessel models, $k = 1, \ldots, N_{wub}$
lbc:	lower body capillaries
lbve:	lower body venule
lbv:	lower body veins
ubc:	upper body capillaries
ubve:	upper body venule
ubv:	upper body veins
ivc:	inferior vena cava
svc:	superior vena cava
pa:	pulmonary artery
pv:	pulmonary vein
ra:	right atria
rv:	right ventricle
la:	left atria
lv:	left ventricle
Trv:	tricuspid valve
Puv:	pulmonary valve
Miv:	mitral valve
Aov:	aortic valve
ao:	aorta artery
3D:	three-dimensional model

Table 1: Glossary of the terms used in Figure 4.

have

$$\frac{\partial Q_{sa,m}}{\partial t} + \frac{\partial}{\partial x}\left(\frac{Q_{sa,m}^2}{A_{sa,m}}\right) = -\frac{A_{sa,m}}{\rho}\frac{\partial P_{sa,m}}{\partial x} - \frac{\pi D_{sa,m}}{\rho}\tau_{osa,m} \quad m = 1, \ldots, N_{sa}, \quad (29)$$

$$\frac{\partial A_{sa,m}}{\partial t} + \frac{\partial Q_{sa,m}}{\partial x} = 0 \quad m = 1, \ldots, N_{sa}, \quad (30)$$

$$P_{sa,m} = P_{\mathrm{o}} + \frac{E_{sa,m}h_{\mathrm{o}sa,m}}{R_{\mathrm{o}sa,m}}\left(\sqrt{\frac{A_{sa,m}}{A_{\mathrm{o}sa,m}}} - 1\right) + \frac{K_{sa,m}h_{\mathrm{o}sa,m}}{R_{\mathrm{o}sa,m}}\frac{1}{2\sqrt{A_{\mathrm{o}sa,m}A_{sa,m}}}\frac{\partial A_{sa,m}}{\partial t} \quad m = 1, \ldots, N_{sa}. \quad (31)$$

In addition, continuity of mass and continuity of pressure are employed to couple the different arterial segments at junctions. Being N_{jn} the total number of juctions with $N_{cg,j}$ arterial segments converging to junction j we have

$$\sum_{n=1}^{N_{cg,j}} Q_{sa|j,n} = 0 \quad j = 1, \ldots, N_{jn}, \quad (32)$$

$$P_{sa|j,n} = P_{sa|j,1} \quad n = 2, \ldots, N_{cg,j} \quad j = 1, \ldots, N_{jn}, \quad (33)$$

where the pair $(Q_{sa|j}, P_{sa|j})$ indicates the restriction of the flow rate and pressure at the junction j.

Arterioles and Capillaries. After the 1D model the arterial segments are coupled to the 0D Windkessel models whose balance equations are given by (5) and (6). This set of arteriole-capillary models contains N_w elements. Then the set of equations for the lower body

Windkessel elements is

$$\frac{dQ_{w,k}}{dt} = \frac{1}{R_{c,k}R_{a,k}C_{a,k}}\left[R_{a,k}C_{a,k}\frac{d}{dt}(P_{w,k}-P_{wlb,k})+(P_{w,k}-P_{wlb,k})-(R_{c,k}+R_{a,k})Q_{w,k}\right] \quad k=1,\dots N_{wlb}, \tag{34}$$

$$Q_{w,k} = Q_{wlb,k} \qquad k=1,\dots N_{wlb}, \tag{35}$$

while for the upper body Windkessel elements it is

$$\frac{dQ_{w,k}}{dt} = \frac{1}{R_{c,k}R_{a,k}C_{a,k}}\left[R_{a,k}C_{a,k}\frac{d}{dt}(P_{w,k}-P_{wub,k})+(P_{w,k}-P_{wub,k})-(R_{c,k}+R_{a,k})Q_{w,k}\right] \quad k=1,\dots N_{wub}, \tag{36}$$

$$Q_{w,k} = Q_{wub,k} \qquad k=1,\dots N_{wub}. \tag{37}$$

In the two equations above $P_{wlb,k}$, $k=1,\dots,N_{wlb}$, and $P_{wub,k}$, $k=1,\dots,N_{wub}$, are the pressure values at the venous side, at the level of the venules. In addition, the pairs $(Q_{w,k},P_{w,k})$, $k=1,\dots,N_w$, are such that

$$Q_{w,k} = Q_{sa|w,k} \quad k=1,\dots,N_w, \tag{38}$$

$$P_{w,k} = P_{sa|w,k} \quad k=1,\dots,N_w, \tag{39}$$

where the pairs $(Q_{sa|w,k},P_{sa|w,k})$, $k=1,\dots,N_w$ are the restrictions of the flow and pressure values coming from the 1D arterial segments which converge at the corresponding Windkessel element k.

Also, $Q_{wlb,k}$, $k=1,\dots N_{wlb}$, and $Q_{wub,k}$, $k=1,\dots N_{wub}$ are the blood outflows through the Windkessel elements in the lower and upper parts of the body, which coincide with the inflows to those Windkessel elements (see equation (6)), denoted by $Q_{w,k}$, $k=1,\dots,N_{wlb}+N_{wub}$.

Lower and Upper Body Venules. The arterioles and capillaries converge to two large subsystems that represent the venous circulation, the lower and the upper parts of the body. Hence, the arteriole-capillary Windkessel models are divided into two subsets, the lower and upper body sets, with N_{wlb} and N_{wub} Windkessel models each, respectively, such that $N_w = N_{wlb}+N_{wub}$. Being $(Q_{wlb,k},P_{wlb,k})$, $k=1,\dots,N_{lb}$ and $(Q_{wub,k},P_{wub,k})$, $k=1,\dots,N_{ub}$, the flow-pressure pair for each Windkessel model, we have that

$$\sum_{k=1}^{N_{wlb}} Q_{wlb,k} = Q_{lbc} \qquad P_{wlb,k} = P_{lbc} \quad k=1,\dots,N_{wlb}, \tag{40}$$

$$\sum_{k=1}^{N_{wub}} Q_{wub,k} = Q_{ubc} \qquad P_{wub,k} = P_{ubc} \quad k=1,\dots,N_{wub}. \tag{41}$$

Then, the venules in the lower and upper parts are modeled using equations (7) and (8), that is

$$L_{lbve}\frac{dQ_{lbve}}{dt} + R_{lbve}Q_{lbve} = P_{lbve} - P_{lbv}, \tag{42}$$

$$C_{lbve}\frac{d}{dt}(P_{lbve} - P_{ex}) = Q_{lbc} - Q_{lbve}, \tag{43}$$

$$L_{ubve}\frac{dQ_{ubve}}{dt} + R_{ubve}Q_{ubve} = P_{ubve} - P_{ubv}, \tag{44}$$

$$C_{ubve}\frac{d}{dt}(P_{ubve} - P_{ex}) = Q_{ubc} - Q_{ubve}. \tag{45}$$

According to the scheme displayed in Figure 4, two more equations are needed to perform the connection between the systemic arteries and the venules, these are

$$P_{lbc} = P_{lbve}, \tag{46}$$

$$P_{ubc} = P_{ubve}. \tag{47}$$

Lower and Upper Body Veins. The veins are, like the venules, modeled using a 0D model described by equations (7) and (8). So, in this case we have

$$L_{lbv}\frac{dQ_{lbv}}{dt} + R_{lbv}Q_{lbv} = P_{lbv} - P_{ivc}, \tag{48}$$

$$C_{lbv}\frac{d}{dt}(P_{lbv} - P_{ex}) = Q_{lbve} - Q_{lbv}, \tag{49}$$

$$L_{ubv}\frac{dQ_{ubv}}{dt} + R_{ubv}Q_{ubv} = P_{ubv} - P_{svc}, \tag{50}$$

$$C_{ubv}\frac{d}{dt}(P_{ubv} - P_{ex}) = Q_{ubve} - Q_{ubv}. \tag{51}$$

Inferior and Superior Vena Cava. The two most important pipes in the venous system are modeled by using the corresponding 0D models as described by equations (7) and (8). Therefore, it is

$$L_{ivc}\frac{dQ_{ivc}}{dt} + R_{ivc}Q_{ivc} = P_{ivc} - P_{ra}, \tag{52}$$

$$C_{ivc}\frac{d}{dt}(P_{ivc} - P_{ex}) = Q_{lbv} - Q_{ivc}, \tag{53}$$

$$L_{svc}\frac{dQ_{svc}}{dt} + R_{svc}Q_{svc} = P_{svc} - P_{ra}, \tag{54}$$

$$C_{svc}\frac{d}{dt}(P_{svc} - P_{ex}) = Q_{ubv} - Q_{svc}. \tag{55}$$

where P_{ra} is the pressure in the right atrium.

Right Atrium and Tricuspid Valve. The first half of the right heart is modeled using the chamber-

valve model presented in equations (9), (14) and (15). Thus, we have

$$P_{ra} - P_{ex} = E_{ra}(t)(V_{ra} - V_{0,ra}) + S_{ra}\frac{dV_{ra}}{dt}, \tag{56}$$

$$\frac{dV_{ra}}{dt} = Q_{ivc} + Q_{svc} - Q_{Trv}, \tag{57}$$

$$L_{Trv}\frac{dQ_{Trv}}{dt} + R_{Trv}Q_{Trv} + B_{Trv}|Q_{Trv}|Q_{Trv} = \Xi_{Trv}(P_{ra} - P_{rv}), \tag{58}$$

$$\Xi_{Trv} = \frac{(1-\cos\theta_{Trv})^4}{(1-\cos\theta_{max,Trv})^4}. \tag{59}$$

where P_{rv} is the pressure in the right ventricle and θ_{Trv} is governed by a set of equations (17).

Right Ventricle and Pulmonary Valve. In the same manner, the second half of the right heart is modeled using equations (9), (14) and (15), such that

$$P_{rv} - P_{ex} = E_{rv}(t)(V_{rv} - V_{0,rv}) + S_{rv}\frac{dV_{rv}}{dt}, \tag{60}$$

$$\frac{dV_{rv}}{dt} = Q_{Trv} - Q_{Puv}, \tag{61}$$

$$L_{Puv}\frac{dQ_{Puv}}{dt} + R_{Puv}Q_{Puv} + B_{Puv}|Q_{Puv}|Q_{Puv} = \Xi_{Puv}(P_{rv} - P_{pa}), \tag{62}$$

$$\Xi_{Puv} = \frac{(1-\cos\theta_{Puv})^4}{(1-\cos\theta_{max,Puv})^4}. \tag{63}$$

where P_{pa} is the pressure in the pulmonary arteries and θ_{Puv} is governed by a set of equations (17).

Pulmonary Arteries and Pulmonary Veins. After the right heart we have the pulmonary circulation, from which the pulmonary arteries and the pulmonary veins are modeled by means of equations (7) and (8), leading to

$$L_{pa}\frac{dQ_{pa}}{dt} + R_{pa}Q_{pa} = P_{pa} - P_{pv}, \tag{64}$$

$$C_{pa}\frac{d}{dt}(P_{pa} - P_{ex}) = Q_{Puv} - Q_{pa}, \tag{65}$$

$$L_{pv}\frac{dQ_{pv}}{dt} + R_{pv}Q_{pv} = P_{pv} - P_{la}, \tag{66}$$

$$C_{pv}\frac{d}{dt}(P_{pv} - P_{ex}) = Q_{pa} - Q_{pv}, \tag{67}$$

where P_{la} is the pressure in the left atrium.

Left Atrium and Mitral Valve. After the pulmonary circulation we find the first half of the

left heart, whose model is the chamber-valve model already presented, that is

$$P_{la} - P_{ex} = E_{la}(t)(V_{la} - V_{0,la}) + S_{la}\frac{dV_{la}}{dt}, \tag{68}$$

$$\frac{dV_{la}}{dt} = Q_{pv} - Q_{Miv}, \tag{69}$$

$$L_{Miv}\frac{dQ_{Miv}}{dt} + R_{Miv}Q_{Miv} + B_{Miv}|Q_{Miv}|Q_{Miv} = \Xi_{Miv}(P_{la} - P_{lv}), \tag{70}$$

$$\Xi_{Miv} = \frac{(1-\cos\theta_{Miv})^4}{(1-\cos\theta_{max,Miv})^4}. \tag{71}$$

where P_{lv} is the pressure in the left ventricle and θ_{Miv} is governed by a set of equations (17).

Left Ventricle and Aortic Valve. Analogously, the remainder part of the left heart is modeled using the same set of equations as before, yielding

$$P_{lv} - P_{ex} = E_{lv}(t)(V_{lv} - V_{0,lv}) + S_{lv}\frac{dV_{lv}}{dt}, \tag{72}$$

$$\frac{dV_{lv}}{dt} = Q_{Miv} - Q_{Aov}, \tag{73}$$

$$L_{Aov}\frac{dQ_{Aov}}{dt} + R_{Miv}Q_{Miv} + B_{Aov}|Q_{Aov}|Q_{Aov} = \Xi_{Aov}(P_{lv} - P_{ao}), \tag{74}$$

$$\Xi_{Aov} = \frac{(1-\cos\theta_{Aov})^4}{(1-\cos\theta_{max,Aov})^4}. \tag{75}$$

where P_{ao} is the pressure in the aortic root and θ_{Aov} is governed by a set of equations (17). Finally, the system is closed by setting

$$Q_{Aov} = Q_{sa,1}, \tag{76}$$

$$P_{ao} = P_{sa,1}, \tag{77}$$

where $(Q_{sa,1}, P_{sa,1})$ is the flow-pressure pair corresponding to the first segment of the set of systemic arteries which stands for the aortic root and ascending aorta.

Specific arterial vessels. For a given 3D model the governing equations are (23)–(28), with the addition of the coupling equations among this 3D model and the 1D model of the arterial tree. These equations are given by

$$Q_{sa|3D,i} = \int_{\Gamma_i} \mathbf{u}_{3D}\cdot\mathbf{n}\, d\Gamma_i \quad i = 1,\dots,N_{cf}, \tag{78}$$

$$P_{sa|3D,i} = ((P_{3D}\mathbf{I} - \mu\nabla\mathbf{u}_{3D})\mathbf{n})_{|\Gamma_i} \quad i = 1,\dots,N_{cf}, \tag{79}$$

where the pairs $(Q_{sa|3D,i}, P_{sa|3D,i})$, $i = 1,\dots,N_{cf}$, denote the restriction of the flow rate and pressure in the systemic arteries which converge to the N_{cf} coupling interfaces of the 3D model.

4 PHYSIOLOGICAL DATA

In this section we collect all the data used in setting the 1D-0D closed-loop model of the cardiovascular system. Also, the sources from which most of the data were taken are given.

The parameters used in the 1D-0D model have been assigned or estimated based on the data reported in Avolio (1980); Liang and Takagi (2009); Heldt et al. (2002); van Heusden et al. (2006); Liang and Liu (2005, 2006); Olufsen et al. (2005); Hoppensteadt and Peskin (2002); Pontrelli (2004). The values of the parameters used in model for the peripheral circulation, the heart model and model of the cardiac valves are given in the tables presented in the forthcoming sections. These values are based on the data reported in Liang and Takagi (2009); Heldt et al. (2002); Hoppensteadt and Peskin (2002).

4.1 Larger arteries

The values for the density and the viscosity of the blood are $\rho = 1.04\,\text{g/cm}^3$ and $\mu = 0.04\,\text{dyn s/cm}^2$, respectively. The parameters used in the 1D model of the arterial tree are according to the model proposed in Avolio (1980), and are repeated here for the sake of completeness in Table 2.

Segment	Description	L [cm]	R_o [cm]	h_o [cm]	$E\left[\frac{\text{dyn}}{\text{cm}^2}\right]$	$k\left[\frac{\text{dyn s}}{\text{cm}^2}\right]$
1	Ascending aorta	4.0	1.45	0.163	4000000	44000
2	Aortic arch	2.0	1.12	0.132	4000000	44000
5	Aortic arch	3.9	1.07	0.127	4000000	44000
11	Thoracic aorta	5.2	1.00	0.120	4000000	44000
21	Thoracic aorta	5.2	0.95	0.116	4000000	44000
34	Thoracic aorta	5.2	0.95	0.116	4000000	44000
50	Abdominal aorta	5.3	0.87	0.108	4000000	44000
65	Abdominal aorta	5.3	0.57	0.080	4000000	44000
75	Abdominal aorta	5.3	0.57	0.080	4000000	44000
49	Coeliac artery	1.0	0.39	0.064	4000000	44000
61	Gastric artery	7.1	0.18	0.045	4000000	44000
62	Splenic artery	6.3	0.28	0.054	4000000	44000
63	Hepatic artery	6.6	0.22	0.049	4000000	44000
64	Renal artery	3.2	0.26	0.053	4000000	44000
66	Superior mesenteric	5.9	0.43	0.069	4000000	44000
67	Gastric artery	3.2	0.26	0.053	4000000	44000
83	Inferior mesenteric	5.0	0.16	0.043	4000000	44000
4	L. common carotid	8.9	0.37	0.063	4000000	44000
10	L. common carotid	8.9	0.37	0.063	4000000	44000
20	L. common carotid	3.1	0.37	0.063	4000000	44000
12	R. common carotid	8.9	0.37	0.063	4000000	44000
22	R. common carotid	8.9	0.37	0.063	4000000	44000
3	L. subclavian artery	3.4	0.42	0.067	4000000	44000
6	Brachiocephalic artery	3.4	0.62	0.086	4000000	44000
82,84	Common iliac	5.8	0.52	0.076	4000000	44000
89,92	External iliac	8.3	0.29	0.055	4000000	44000
90,91	Internal iliac	5.0	0.20	0.040	16000000	178000
98,99	External iliac	6.1	0.27	0.053	4000000	44000
104,107	Femoral artery	12.7	0.24	0.050	8000000	89000
105,106	Profundis artery	12.6	0.23	0.049	16000000	178000
109,110	Femoral artery	12.7	0.24	0.050	8000000	89000
111,112	Popliteal artery	9.4	0.20	0.047	8000000	89000
113,114	Popliteal artery	9.4	0.20	0.050	4000000	44000
115,118	Anterior tibial artery	2.5	0.13	0.039	16000000	178000
119,124	Anterior tibial artery	15.0	0.10	0.020	16000000	178000
125,128	Anterior tibial artery	15.0	0.10	0.020	16000000	178000
116,117	Posterior tibial artery	16.1	0.18	0.045	16000000	178000
121,122	Posterior tibial artery	16.1	0.18	0.045	16000000	178000
120,123	Peroneal artery	15.9	0.13	0.039	16000000	178000
126,127	Peroneal artery	15.9	0.13	0.019	16000000	178000

Table 2: Geometric and mechanical parameters of the arterial segments.

Segment	Description	L [cm]	R_{o} [cm]	h_{o} [cm]	$E\ \left[\frac{\mathrm{dyn}}{\mathrm{cm}^2}\right]$	$k\ \left[\frac{\mathrm{dyn\,s}}{\mathrm{cm}^2}\right]$
31,37	Carotid (internal)	5.9	0.18	0.045	8000000	89000
32,36	External carotid	11.8	0.15	0.042	8000000	89000
33,35	Superior thyroid artery	4.0	0.07	0.020	8000000	89000
43,56	Lingual artery	3.0	0.10	0.030	8000000	89000
44,55	Internal carotid	5.9	0.13	0.039	8000000	89000
45,54	Facial artery	4.0	0.10	0.030	16000000	178000
46,53	Middle cerebral	3.0	0.06	0.020	16000000	178000
47,52	Cerebral artery	5.9	0.08	0.026	16000000	178000
48,51	Opthalmic artery	3.0	0.07	0.020	16000000	178000
60,68	Internal carotid	5.9	0.08	0.026	16000000	178000
73,77	Superficial temporal	4.0	0.06	0.020	16000000	178000
74,76	Maxilliary artery	5.0	0.07	0.020	16000000	178000
7,15	Internal mammary	15.0	0.10	0.030	8000000	89000
8,14	Subclavian artery	6.8	0.40	0.066	4000000	44000
9,13	Vertebral artery	14.8	0.19	0.045	8000000	89000
16,26	Costo-cervical artery	5.0	0.10	0.030	8000000	89000
17,25	Axilliary artery	6.1	0.36	0.062	4000000	44000
18,24	Suprascapular	10.0	0.20	0.052	8000000	89000
19,23	Thyrocervical	5.0	0.10	0.030	8000000	89000
27,41	Thoraco-acromial	3.0	0.15	0.035	16000000	178000
28,40	Axilliary artery	5.6	0.31	0.057	4000000	44000
29,39	Circumflex scapular	5.0	0.10	0.030	16000000	178000
30,38	Subscapular	8.0	0.15	0.035	16000000	178000
42,57	Brachial artery	6.3	0.28	0.055	4000000	44000
58,70	Profunda brachi	15.0	0.15	0.035	8000000	89000
59,69	Brachial artery	6.3	0.26	0.053	4000000	44000
71,79	Brachial artery	6.3	0.25	0.052	4000000	44000
72,78	Superior ulnar collateral	5.0	0.07	0.020	16000000	178000
80,86	Inferior ulnar collateral	5.0	0.06	0.020	16000000	178000
81,85	Brachial artery	4.6	0.24	0.050	4000000	44000
87,94	Ulnar artery	6.7	0.21	0.049	8000000	89000
88,93	Radial artery	11.7	0.16	0.043	8000000	89000
95,102	Ulnar artery	8.5	0.19	0.046	8000000	89000
96,101	Interossea artery	7.9	0.09	0.028	16000000	178000
97,100	Radial artery	11.7	0.16	0.043	8000000	89000
103,108	Ulnar artery	8.5	0.19	0.046	8000000	89000

Table 2: Geometric and mechanical parameters of the arterial segments.

4.2 Arterioles and Capillaries

The parameters that characterize the behavior of the arterioles and capillaries through the Windkessel element have been computed according to the guidelines provided in Stergiopulos et al. (1992), and are given in Table 3.

Terminal	R_c	R_a	C_a
	$\left[\frac{\text{dyn s}}{\text{cm}^2\,\text{ml}}\right]$		$\left[\frac{\text{ml cm}^2}{\text{dyn}}\right]$
125128	62781.6	251356	1.00E-006
126127	31792.6	127400	1.00E-006
121122	21693	86769.2	2.00E-006
105106	12280.8	49008.4	4.00E-006
90,91	15724.8	62781.6	3.00E-006
83	31103.8	125104	2.00E-006
64	3971.8	15839.6	1.20E-005
66	3329.2	13314	1.40E-005
67	3971.8	15839.6	1.20E-005
61	23758	94918.6	2.00E-006
62	8608.6	34433	5.00E-006
63	6851.6	27431.6	7.00E-006
9,13	22037.4	88032	2.00E-006
7,15	89409.6	358092	1.00E-006
19,23	89409.6	358092	1.00E-006
18,24	20774.6	83326.6	2.00E-006
16,26	89409.6	358092	1.00E-006

Terminal	R_c	R_a	C_a
	$\left[\frac{\text{dyn s}}{\text{cm}^2\,\text{ml}}\right]$		$\left[\frac{\text{ml cm}^2}{\text{dyn}}\right]$
30,38	84015.4	198562	1.00E-006
29,39	126252	506156	0.00E+000
27,41	84015.4	198562	1.00E-006
58,70	35120.4	140280	1.00E-006
72,78	252504	1007720	0.00E+000
80,86	370720	1480640	0.00E+000
97,100	33055.4	131990.6	1.00E-006
96,101	159530	635852	0.00E+000
103,108	22265.6	89065.2	2.00E-006
33,35	44303	176750	1.00E-006
48,51	62666.8	250208	1.00E-006
47,52	51189.6	204302	1.00E-006
46,53	92163.4	368424	1.00E-006
43,56	22265.6	88950.4	2.00E-006
45,54	31448.2	126252	1.00E-006
74,76	62666.8	250208	1.00E-006
73,77	92163.4	368424	1.00E-006

Table 3: Windkessel terminals corresponding to each arterial segment (for numbers see Table 2).

4.3 Venules, veins and inferior and superior vena cava

The elements of the 0D model for the venous system are callibrated using the data provided in Table 4.

	Lower body			Upper body		
	Venules	Veins	Inferior cava	Venules	Veins	Superior cava
R [dyn cm^{-2} s ml^{-1}]	53.32	11.997	0.6665	186.62	39.99	0.6665
L [dyn cm^{-2} s^2 ml^{-1}]	1.333	0.6665	0.6665	1.333	0.6665	0.6665
C [ml dyn^{-1} cm^2]	0.00112528	0.05626407	0.01125281	0.00037509	0.01125281	0.00375094

Table 4: Data used in the 0D model of the venous circulation system.

4.4 Right and left hearts

The data for the elastance model of the right and left hearts as well as the data needed by the model for the valves are provided in Table 5 and Table 6. The cardiac cycle is defined with a period $T = 1$ s.

Chambers	Right atrium	Right ventricle	Left atrium	Left ventricle
E_A [dyn cm^{-2} ml^{-1}]	79.98	733.15	93.31	3665.75
E_B [dyn cm^{-2} ml^{-1}]	93.31	66.65	119.97	106.64
T_c [s]	0.17	0.34	0.17	0.34
T_r [s]	0.17	0.15	0.17	0.15
t_c [s]	0.80	–	0.80	–
t_r [s]	0.97	–	0.97	–
V_0 [ml]	4.0	10.0	4.0	5.0
α	0.0005	0.0005	0.0005	0.0005

Table 5: Data used in the elastance model of the right and left halves of the heart.

Valves	Tricuspid	Pulmonar	Mitral	Aortic
R [dyn cm^{-2} s ml^{-1}]	0.006	0.006	0.006	0.006
L [dyn cm^{-2} s^2 ml^{-1}]	0.005	0.005	0.005	0.005
B [dyn cm^{-2} s^2 ml^{-2}]	0.0064	0.00756	0.0064	0.00756
θ_{max} [$^\circ$]	75.0	75.0	75.0	75.0
θ_{min} [$^\circ$]	5.0	5.0	5.0	5.0
k_P/I [rad s^{-2} dyn^{-1} cm^2]	4.126032	4.126032	4.126032	4.126032
k_F/I [s^{-1}]	50.0	50.0	50.0	50.0
k_Q/I [rad s^{-1} ml^{-1}]	2.0	2.0	2.0	2.0
k_V/I [rad s^{-1} ml^{-1}]	3.5	3.5	3.5	7.0

Table 6: Data used in the non-ideal diode models of the cardiac valves.

4.5 Pulmonary arteries and veins

The data for the 0D models that represent the both the pulmonary arteries and veins are given in Table 7.

	Pulmonary arteries	Pulmonary veins
R [dyn cm^{-2} s ml^{-1}]	106.64	13.33
L [dyn cm^{-2} s^2 ml^{-1}]	0.0	0.0
C [ml dyn^{-1} cm^2]	0.00309077	0.060015

Table 7: Data used in the 0D models for the compartments in the pulmonary circulation.

4.6 Specific vessels

The geometrical data corresponding to set up three-dimensional models of arterial vessels is obtained either by resorting to a standard geometry or to medical images. This will be clear in each specific example. In the case of patient-specific vessels, the extraction of the anatomical structures is done following standard steps for the segmentation of the medical images.

Regarding mechanical parameters (E and k in equation (26)) the arterial wall parameters in the 3D model match those pertaining to the 1D model in which the specific vessel is embedded. As for the values for the density and the viscosity of the blood, as with the 1D model, we take $\rho = 1.04$ g/cm^3 and $\mu = 0.04$ dyn s/cm^2, respectively.

5 CARDIOVASCULAR SIMULATIONS

5.1 Numerical approximation

The numerical approximation of the model for the arterial tree network, eventually with an embedded 3D model, is carried out as in Urquiza et al. (2006); Blanco et al. (2007). The discretization of the 0D models is done following a second order Crank-Nicolson method combined with fixed point iterations for dealing with the non-differentiable non-linearity of the valve models.

5.2 Case 1: 1D-0D closed-loop model

In this first case we employ the 1D-0D closed-loop model (no 3D model is considered here). All the parameters for the standard case are those given in Section 4. Whenever a parameter is changed it is specified.

Figure 5 summarizes provides the results in several points throughout the cardiovascular system. These results are in accordance with patient-specific records published in the literature.

Figure 6 shows the flow rate and the opening angle in each one of the four cardiac valves. Observe that the dynamics is not described by a mere binary state. As well, as discussed in

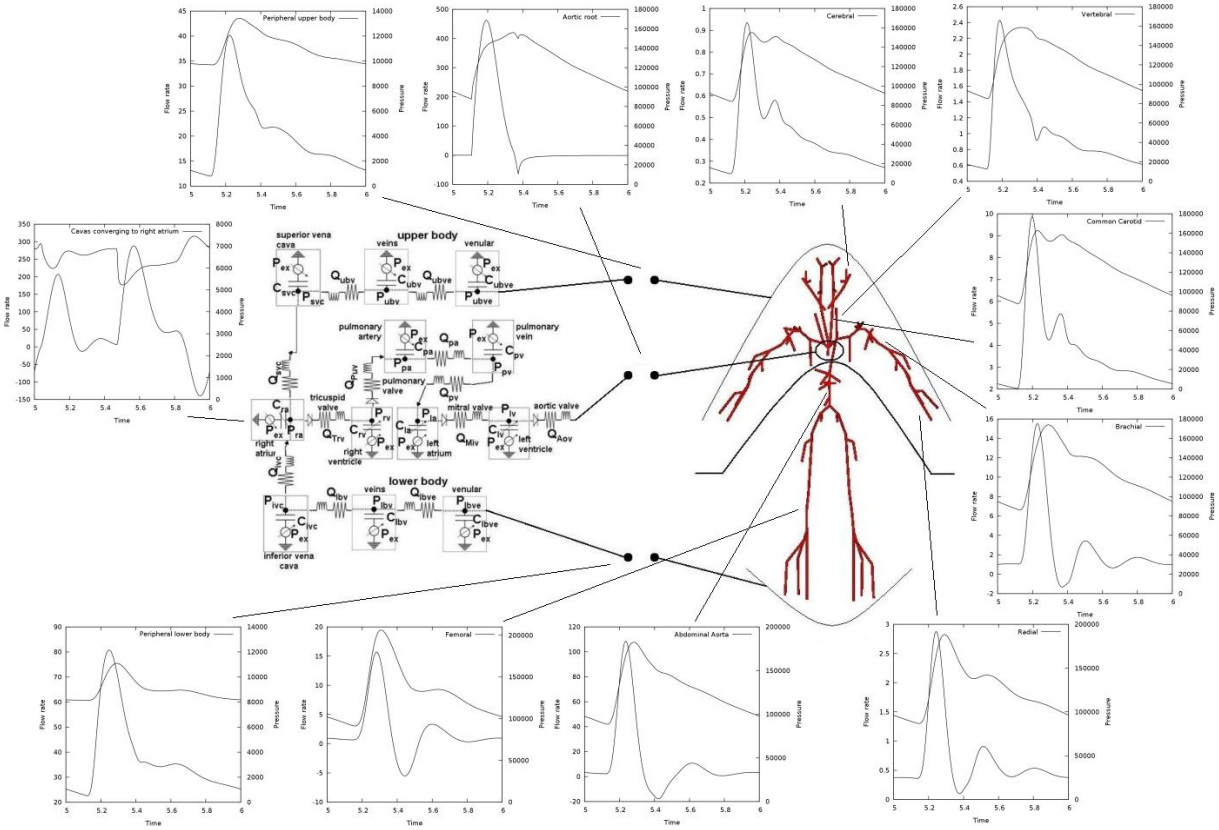

Figure 5: Results throughout the entire 1D-0D cardiovascular model.

Korakianitis and Shi (2006), the results given by this model with respect to the opening angle are in agreement with data reported in the literature concerning valve dynamics.

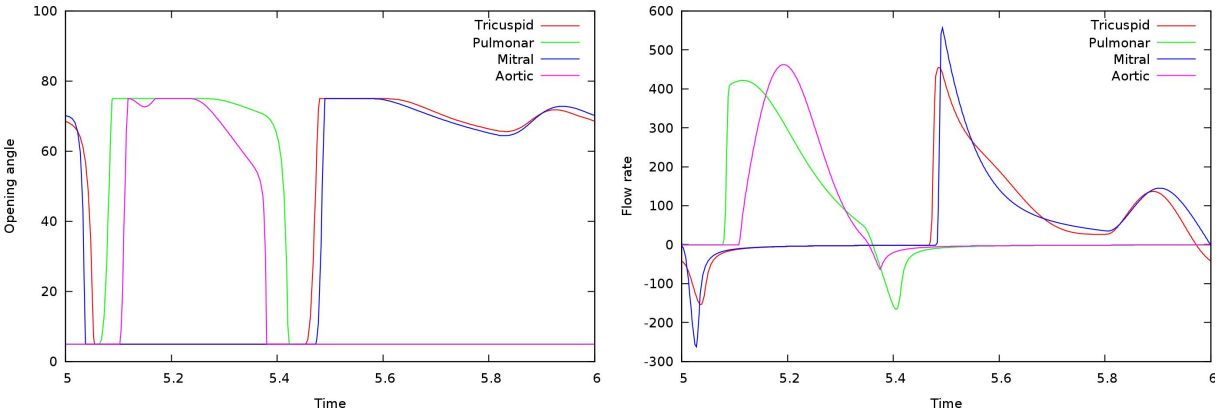

Figure 6: Opening angle and flow rate in the four cardiac valves.

In turn, Figure 7 displays the vole and the pressure in each cardiac chamber. It is worth saying that the present model is still under calibration using either data reported in the literature as well as patient-specific measurements in order to improve the results obtained from the simulations.

Now we simulate the case in which we have a regurgitant aortic valve with different disease severities. The interested reader is referred to Korakianitis and Shi (2006) for an exhaustive discussion on this topic, recalling that there the authors make use of a lumped model for the systemic arteries. We concentrate here on studying the sensitivity of the results when changing

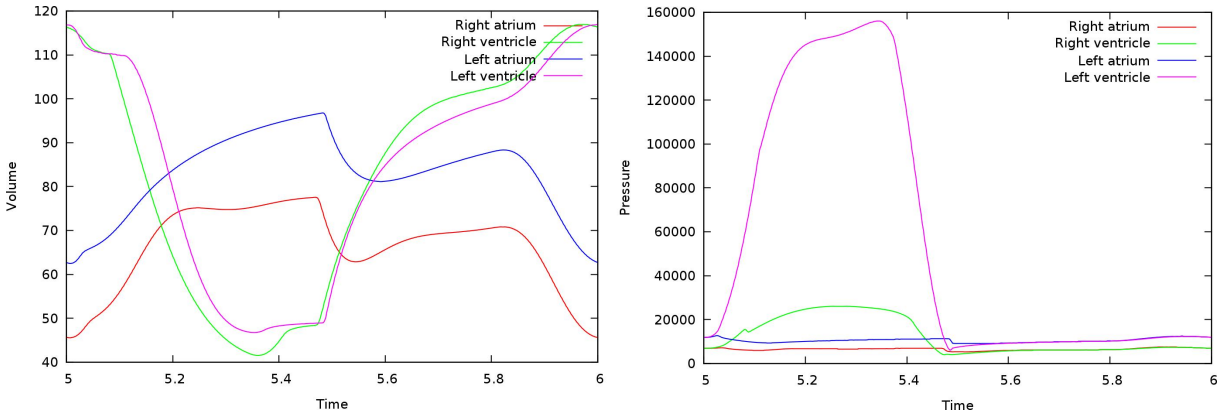

Figure 7: Volume and pressure in the four cardiac chambers.

the severity of the disease. The regurgitant aortic valve is modelled by increasing the minimum angle the valve is able to reach. The range tested here is $\theta_{min,Aov} \in \{15°, 20°, 25°, 30°\}$ (see Table 6).

In all the simulations no auto-regulatory mechanism has been taken into account, noting that this is relevant for the correct description of the problem since the control mechanism play a main role in re-establishing the pressure to physiological values.

In Figures 8- 11 we address the response of the system at several points. Figure 8 shows a notorious decrease in the left ventricle pressure during early systole, provoking the early opening of the aortic valve as seen also in that figure. In turn, the regurgitation in the aortic valve does not affect the dynamics of the mitral valve (opening angle) as shown in Figure 9. Nevertheless it affects the pressure in the right atrium, increasing its value.

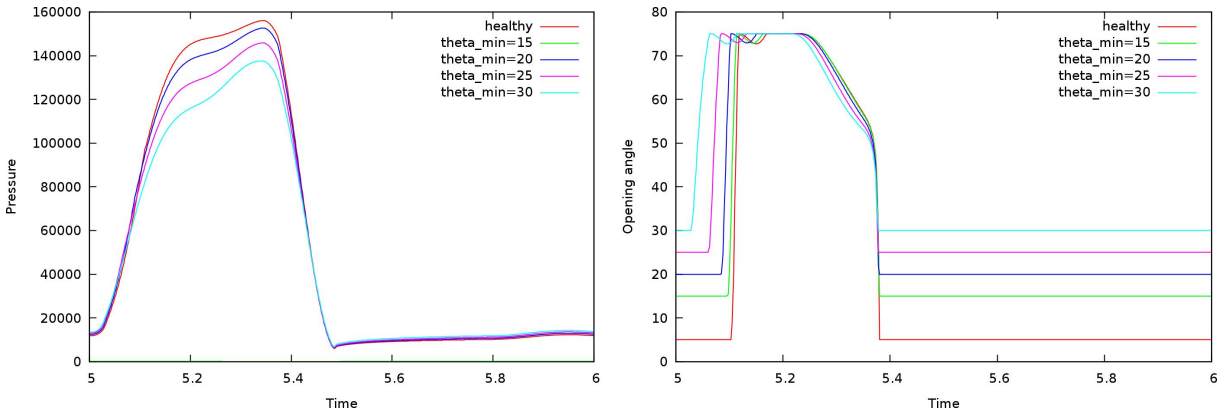

Figure 8: Comparison at the left ventricle between healthy and regurgitant aortic valve.

Concerning the resuls in the systemic arteries (specifically at the aortic root), Figures 10 and 11 present the flow rate and the pressure at the aortic root and at the common carotid artery, respectively. In Figure 10 the decrease in the diastolic pressure is significant, result of the valve insufficiency. Observe that the flow at the common carotid decreases to a point in which is becomes negative during diastole (due to the lack of auto-regulation in the system). Both figures also evince the decrease in the pressure during early systole, as with the pressure at the left ventricle. The lack of increase in the systolic pressure can be justified as a result of the lack for autoregulation in the cardiovascular system. It is easy to see that if such mechanisms are present, then they push the system back to a physiological mean pressure. Now, since the

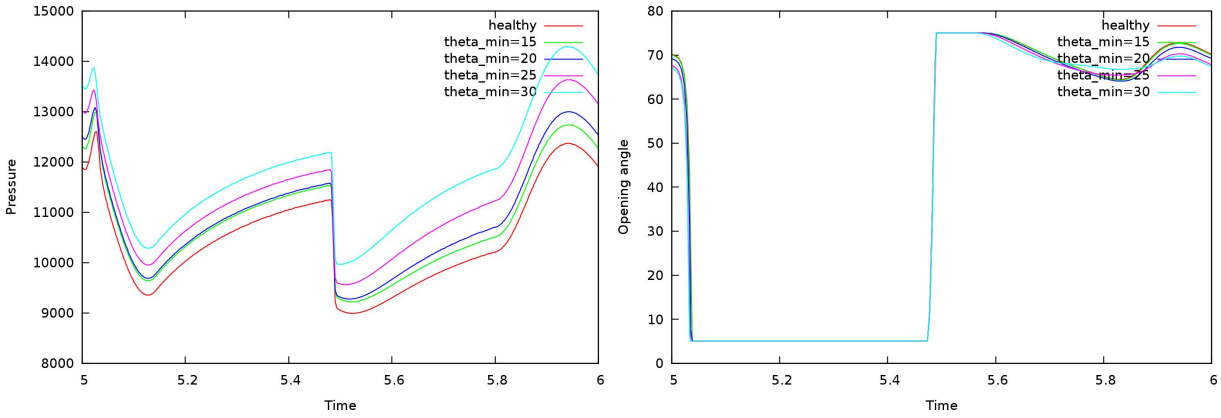

Figure 9: Comparison at the left atrium (and mitral valve) between healthy and regurgitant aortic valve.

systole-to-diastole pressure drop has been increased we would have an increased value of the pressure during systole and a decreased value during diastole.

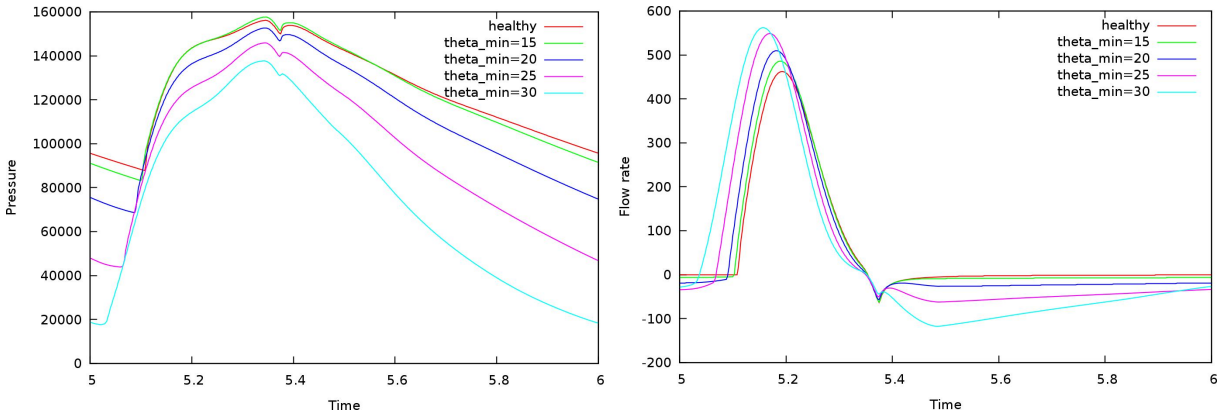

Figure 10: Comparison at the aortic root between healthy and regurgitant aortic valve.

5.3 Case 2: 3D-1D-0D closed-loop model

In this example we introduce a patient-specific cerebral aneurism into the 1D-0D closed-loop model for the cardiovascular system and performa simulation accounting for all the phenomena discussed in the preeceding sections. Schematically, we have the situation shown in Figure 12.

Figure 13 presents the flow rate and the pressure at the proximal coupling interface. This solution matches the one obtained with the pure 1D model, wchich means that replacing the small 1D piece by a 3D counterpart (including an aneurism) is not visible from the global hemodynamics viewpoint.

As well, we present in Figure 14 the streamlines within the 3D domain as the result of the interaction between the 3D model and the closed-loop system. Evidently, with such an approach it is possible to set up quite general cardiovascular scenarios. The sensitivity of the hemodynamics at this aneurism with respect to global factors is something that may help in answering questions about the influence of global variables, such as heart rate, peripheral resistance, mean pressure, to local hemodynamics indexes which are believed to be connected with aneurysm rupture. No further comment is made here, since the discussion of these results is out of the scope of the present work.

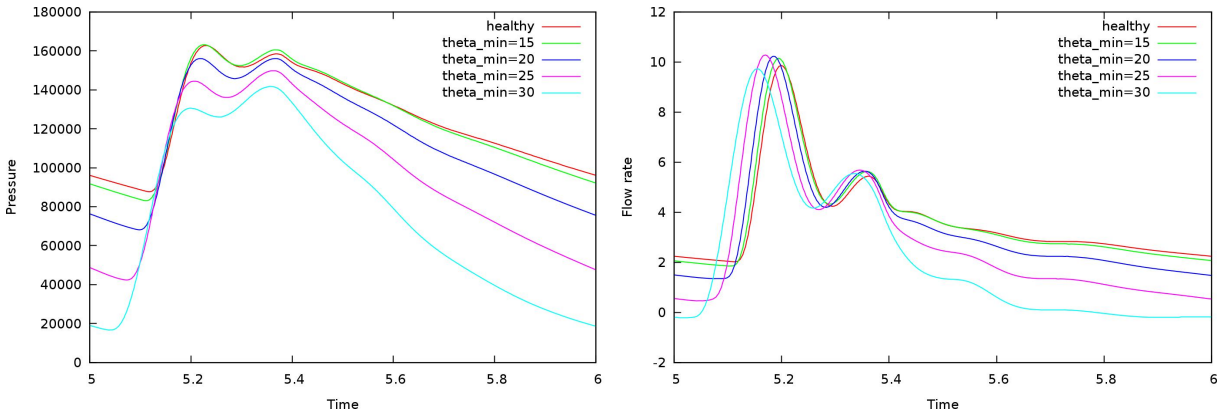

Figure 11: Comparison at the common carotid artery between healthy and regurgitant aortic valve.

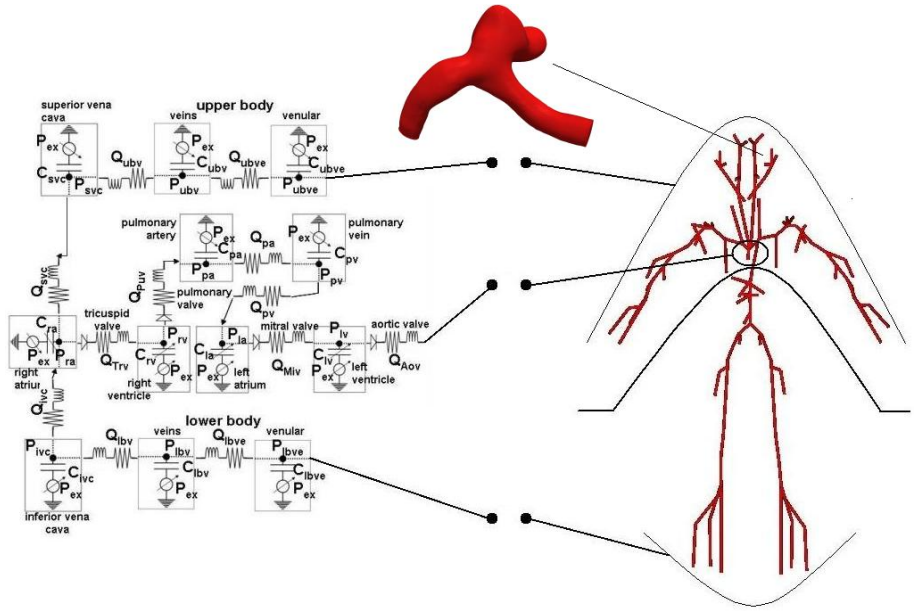

Figure 12: Scheme of the 1D-0D closed-loop model with a 3D patient-specific aneurism embedded in it.

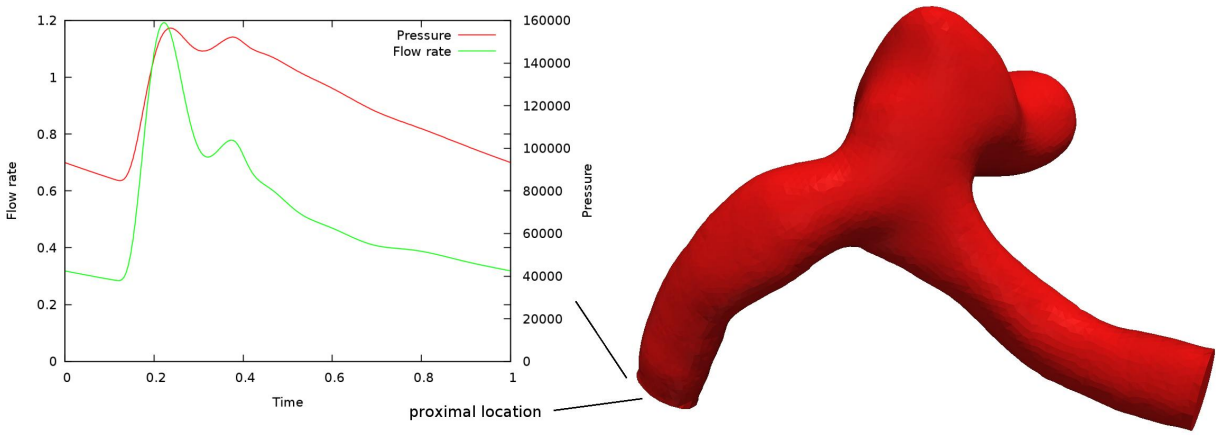

Figure 13: Pressure and flow rate at the proximal coupling interface.

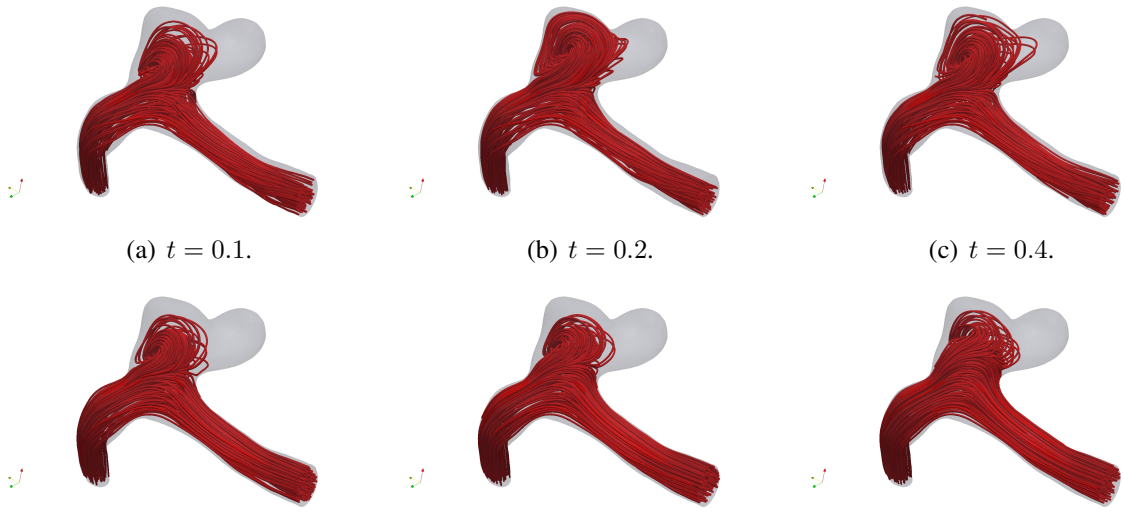

(a) $t = 0.1$. (b) $t = 0.2$. (c) $t = 0.4$.

(d) $t = 0.6$. (e) $t = 0.8$. (f) $t = 1.0$.

Figure 14: Streamlines at different instants throughout one cardiac cycle.

6 CONCLUSIONS

In this paper we have presented an integrative model of the cardiovascular system coupling different levels of circulation, ranging from the arterial/venous circulation to blood flow in specific vessels, accounting also for the peripheral circulation and non-ideal valve functioning.

This work comprises a step towards establishing a quite complex model which allows to analyze the interplay among several factors that render the closed-loop behavior of the cardiovascular system such as the arterial/venous coupling, the local/global hemodynamics and cardiac/arterial interactions, among others. With this kind of models it is possible to reach a truly wide range of physiological and pathofisiological scenarios being characterized by either global and local changes in the cardiovascular state.

A simple example of aortic valve regurgitation was addressed, and the sensitivity with respect to the insufficiency severity and its impact in terms of hemodynamics variables was briefly discussed. As seen in this analysis, further work is needed to incorporate to the present model homeostatic mechanisms like baroreflex or chemoreflex in order to incorporate the possibility of auto-regulation in the cardiovascular system.

Finally, with the present model a truly 3D-1D-0D simulation in the physiological regime was presented for the case of a patient-specific aneurism embedded in the 1D-0D closed-loop model for the cardiovascular system.

REFERENCES

Avolio A. Multi-branched model of the human arterial system. *Med. Biol. Engrg. Comp.*, 18:709–718, 1980.

Blanco P., Feijóo R., and Urquiza S. A unified variational approach for coupling 3D-1D models and its blood flow applications. *Comp. Meth. Appl. Mech. Engrg.*, 196:4391–4410, 2007.

Blanco P., Pivello M., Urquiza S., and Feijóo R. On the potentialities of 3D–1D coupled models in hemodynamics simulations. *J. Biomech.*, 42:919–930, 2009.

Blanco P., Urquiza S., and Feijóo R. Assessing the influence of heart rate in local hemodynamics through coupled 3D-1D-0D models. *Int. J. Num. Meth. Biomed. Engng.*, 26:890–903, 2010.

Formaggia L., Gerbeau J.F., Nobile F., and Quarteroni A. On the coupling of

3D and 1D Navier-Stokes equations for flow problems in compliant vessels. *Comp. Meth. Appl. Mech. Engrg.*, 191:561–582, 2001.

Grinberg L., Anor T., Madsen J., Yakhot A., and Karniadakis G. Large-scale simulation of the human arterial tree. *Clinical and Experimental Pharmacology and Physiology*, 36:194–205, 2009.

Heldt T., Shim E., Kamm R., and Mark R. Computational modeling of cardiovascular response to orthostatic stress. *J. Appl. Physiol.*, 92:1239–1254, 2002.

Hoppensteadt F. and Peskin C. *Modeling and Simulation in Medicine and the Life Sciences*. Texts in Applied Mathematics, Springer, 2002.

Hughes T. *A Study of the One-Dimensional Theory of Arterial Pulse Propagation*. Ph.D. thesis, University of California, Berkeley, 1974.

Kim H., Vignon-Clementel I., Figueroa C., LaDisa J., Jansen K., Feinstein J., and Taylor C. On coupling a lumped parameter heart model and a three-dimensional finite element aorta model. *Ann. Biomed. Engng.*, 37:2153–2169, 2009.

Kivity Y. and Collins R. Nonlinear fluid-shell interactions: application to blood flow in large arteries. *Int. Sym. Discrete Meth. Engrg.*, pages 476–488, 1974a.

Kivity Y. and Collins R. Nonlinear wave propagation in viscoelastic tubes: application to aortic rupture. *J. Biomech.*, pages 67–76, 1974b.

Korakianitis T. and Shi Y. Numerical simulation of cardiovascular dynamics with healthy and diseased heart valves. *J. Biomech.*, 39:1964–1982, 2006.

Kufahl R. and Clark M. A circle of willis simulation using distensible vessels and pulsatile flow. *J. Biomech. Engrg.*, 107:112–122, 1985.

Lanzarone E., P.Liani, and aand M.L. Constantino G.B. Model of arterial tree and peripheral control for the study of physiological and assisted circulation. *Medical Engineering and Physics*, 29:542–555, 2007.

Liang F. and Liu H. A closed-loop lumped parameter computational model for human cardiovascular system. *JSME International Journal*, 48:Series C, 2005.

Liang F. and Liu H. Simulation of hemodynamic responses to the valsalva maneuver: An integrative computational model of the cardiovascular system and the autonomic nervous system. *J. Physiol. Sci.*, 56:45–65, 2006.

Liang F. and Takagi S. Multi-scale modeling of the human cardiovascular system with applications to aortic valvular and arterial stenoses. *Med. Biol. Eng. Comput.*, 47:743–755, 2009.

Migliavacca F., Balossino R., Pennati G., Dubini G., Hsia T.Y., de Leval M., and Bove E. Multiscale modelling in biofluidynamics: Application to reconstructive paediatric cardiac surgery. *J. Biomech.*, 39:1010–1020, 2006.

Olufsen M., Ottesen J., Tran H., Ellwein L., Lipsitz L., and Novak V. Blood pressure and blood flow variation during postural change from sitting to standing: model development and validation. *J. Appl. Physiol.*, 99:1523–1537, 2005.

Olufsen M., Peskin C., Kim W., Pedersen E., Nadim A., and Larsen J. Numerical simulation and experimental validation of blood flow in arteries with structured-tree outflow conditions. *Ann. Biomed. Engng.*, 28:1281–1299, 2000.

Pontrelli G. A multiscale approach for modelling wave propagation in an arterial segment. *Comp. Meth. Biomech. Biom. Engrg.*, 7:79–89, 2004.

Reichold J., Stampanoni M., Keller A., Buck A., Jenny P., and Weber B. Vascular graph model to simulate the cerebral blood flow in realistic vascular networks. *J. Cereb. Blood Flow Metab.*, 29:1429–1443, 2009.

Reymond P., Merenda F., Perren F., Rüfenacht D., and Stergiopulos N. Validation of a one-

dimensional model of the systemic arterial tree. *Am. J. Physiol. Heart Circ. Physiol.*, 297:H208–H222, 2009.

Schaaf B. and Abbrecht P. Digital computer simulation of systemic arterial pulse wave transmission: a nonlinear model. *J. Biomech. Engrg.*, 5:345–364, 1972.

Spencer M. and Deninson A. The square-wave electro-magnetic flowmeter. Theory of operation and design of magnetic probes for clinical and experimental applications. *I.R.E. Trans. Med. Elect.*, 6:220–228, 1959.

Stergiopulos N., Young D., and Rogge T. Computer simulation of arterial flow with applications to arterial and aortic stenoses. *J. Biomech.*, 25:1477–1488, 1992.

Stettler J., Niederer P., and Anliker M. Theoretical analysis of arterial hemodynamics including the influence of bifurcations, part I. *Ann. Biomed. Engrg.*, 9:145–164, 1981.

Urquiza S., Blanco P., Vénere M., and Feijóo R. Multidimensional modeling for the carotid blood flow. *Comp. Meth. Appl. Mech. Engrg.*, 195:4002–4017, 2006.

van Heusden K., Gisolf J., Stok W., Dijkstra S., and Karemaker J.M. Mathematical modeling of gravitational effects on the circulation: importance of the time course of venous pooling and blood volume changes in the lungs. *Am J. Physiol. Heart Circ. Physiol.*, 291:H2152–H2165, 2006.

Vignon-Clementel I., Figueiroa C., Jansen K., and Taylor C. Outflow boundary conditions for three-dimensional finite element modeling of blood flow and pressure waves in arteries. *Comp. Meth. Appl. Mech. Engrg.*, 195:3776–3996, 2006.

Wang J. and Parker K. Wave propagation in a model of the arterial circulation. *J. Biomech.*, 37:457–470, 2004.